THE PENNSYLVANIA STATE UNIVERSITY
SCHREYER HONORS COLLEGE

DEPARTMENT OF CHEMICAL ENGINEERING

DEVICE PERFORMANCE OF POLY(3-HEXYLTHIOPHENE)/FULLERENE SOLAR CELLS IS LIMITED BY ELECTRON TRANSPORT

BRYCE ISAIAH EDMONDSON
FALL 2013

A thesis
submitted in partial fulfillment
of the requirements
for a baccalaureate degree in Chemical Engineering
with honors in Chemical Engineering

Reviewed and approved* by the following:

Enrique D. Gomez
Assistant Professor of Chemical Engineering
Thesis Supervisor and Honors Adviser

Darrell Velegol
Distinguished Professor of Chemical Engineering
Faculty Reader

* Signatures are on file in the Schreyer Honors College.

ABSTRACT

Polythiophene/fullerene mixtures are studied heavily for their application in organic photovoltaic devices. Evidence shows that performance of organic photovoltaics is dependent on the morphology of the active layer at multiple length scales. Nevertheless, the critical morphological parameters governing device performance have not been identified in one of the most studied systems to date, mixtures of regioregular poly(3-hexylthiophene) (P3HT) with [6,6]-phenyl-C_{61}-butyric methyl ester (PCBM). We have examined the role that morphology plays on device performance and find that phase separation within fullerene-rich domains in P3HT/PCBM active layers can strongly affect device performance. Specifically, we have modulated the composition of the fullerene-rich domains by mixing regioregular P3HT, regiorandom P3HT (which is amorphous) and PCBM. We find that replacing regioregular P3HT with regiorandom P3HT has little effect on device performance when spinodal decomposition driven phase separation occurs in the amorphous phases of P3HT/PCBM mixtures. This is consistent with our previous work on characterizing electron transport in amorphous P3HT/PCBM mixtures, where we demonstrate that electron mobilities can vary by orders of magnitude with PCBM composition and is high when phase separation is present.

TABLE OF CONTENTS

LIST OF FIGURES

ACKNOWLEDGEMENTS

I would like to thank all of the brilliant folks of the Gomez lab that have helped me along during my first journey into the world of research. The past three years of lab experience with the graduate students and fellow undergraduate colleagues have taught me more about chemical engineering and research than I could have ever hoped to achieve on my own or through a classroom. Above all, I have come to appreciate how much greater the potential of teamwork is than the potential of one individual. I will always view the work contained within this manuscript as a product of all the individuals that have helped push me along and I am in their debt for the knowledge they have imparted to me.

I must particularly express my immense appreciation for Enrique Gomez as an invaluable adviser throughout this study as well as my entire undergraduate career. Never before have I encountered someone who can so easily communicate knowledge and motivation to others and is so eager to do so. The successes I have seen during the past few years are no doubt a testament to Enrique's ability as a teacher and mentor, and I hope to one day inspire others as he has inspired me.

Finally, though certainly not least of all, I would like to thank my family, friends, and loved ones for their unwavering encouragement. I have found myself leaning on this support many times and cannot express enough gratitude for their confidence in me. Lastly, to the one who has taken this journey with me and endured my stresses alongside me: you know who you are, and I could not have made it to where I am today without you.

Chapter 1

Introduction

Polythiophene/fullerene blends are studied heavily for their application as active layers in organic photovoltaic devices (OPVs). This type of electron donor/acceptor mixture offers the possibility for flexible thin-film solar cells to provide inexpensive and widespread energy.[1-4] Many works have characterized the intricate balance between morphology of the OPV active layer and the device performance. Specifically, a balance between electron donor/acceptor interface for effective charge separation, bicontinuous regions for ease of charge transport, and domain sizes near the exciton diffusion length (5-10nm[5,6]) for reduction of exciton decay, is vital to the efficiency of the device.[7-13] Recent efforts have illustrated the critical morphological dependence on polymer crystallization for polythiophene/fullerene blends and the implications that miscibility has on charge transport of the active layer.[9-10] These efforts have shown that molecular mixing for both semi-crystalline and amorphous regions of the active layer plays a vital role in device performance. However, a clear distinction between the role of molecular mixing and device performance has not yet been identified.

To this end, we have examined the role that morphology plays on device performance by modulating the composition of fullerene-rich domains with mixtures of regioregular poly(3-hexylthiophene-(2,5)-diyl) (RR P3HT), regiorandom P3HT (RRa P3HT), and [6,6]-phenyl-C_{61}-butyric methyl ester (PCBM). Solution processing of these devices allows us to predict the morphology of the active layer based on the morphology of the incipient solution via Flory-Huggins solution theory. **Figure 1-1**, adapted from Kozub *et al.*, depicts the phase diagram expected for solutions of amorphous P3HT and PCBM from this model.[9] High volume fractions

of P3HT indicate a region of miscibility with the fullerene while spinodal decomposition driven phase separation occurs for mixtures with high PCBM content. The Flory-Huggins interaction parameter for P3HT/PCBM, χ, indicates P3HT/PCBM blends enter into the 2-phase regime at $\phi_{P3HT} = 0.42$.

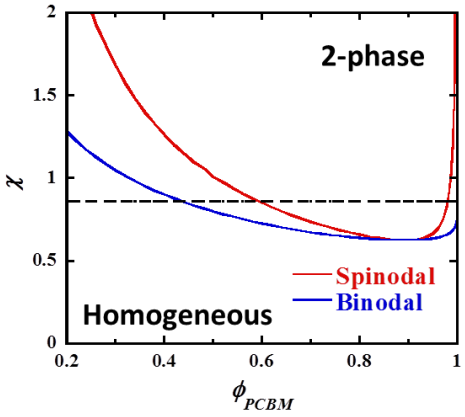

Figure 1-1. Phase diagram for amorphous P3HT/PCBM mixtures. The dashed line indicates the interaction parameter, χ = 0.86, and shows that phase separation occurs at $\phi_{P3HT} = 0.42$ ($\phi_{PCBM} = 0.58$).[9]

Based on the predictions available to us through this analysis, we can propose an initial hypothesis for the introduction of RRa P3HT (amorphous) to the fullerene rich domains of the OPV devices under study. **Figure 1-2**, retrieved from Vakhshouri *et al.*, shows the effect that miscibility or phase separation have on charge mobility through the active layer. When PCBM composition is high and phase separation is present, charge transport plateaus at values that are orders of magnitude greater than those for which RRa P3HT content is high and mixtures are miscible. Thus, we can surmise that when RR P3HT is present and RRa P3HT is introduced to the PCBM matrix surrounding the crystalline polymer, electron transport should be affected heavily depending on the RRa P3HT:PCBM composition. Again, this is examined by observing the device performance for a variety of P3HT:PCBM compositions as well as RR:RRa compositions to determine the interplay between the crystalline polymer and amorphous domain of RRa P3HT and PCBM.

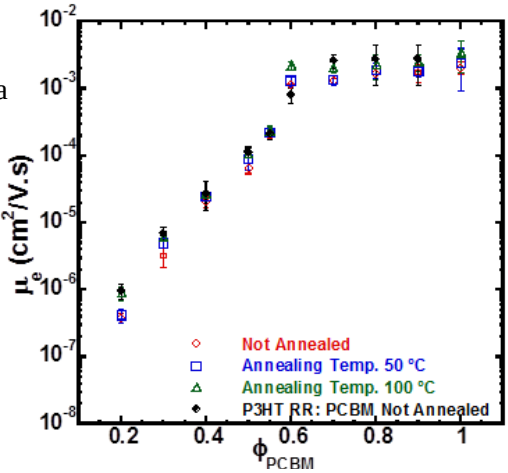

Figure 1-2. Charge mobility as a function of PCBM composition. Mobility is low for low PCBM content and increases to a plateau beginning at $\phi_{PCBM} = 0.6$, a point that correlates to phase separation for the polymer/fullerene blend.

Chapter 2

Experimental Methods

Solutions of regioregular P3HT (96% H-T regioregular, M_n = 28 kg/mol, polydispersity = 1.9, Merck), regiorandom P3HT (M_n = 30 kg/mol, polydispersity = 3, Sigma-Aldrich) and PCBM (>99.5%, Nano-C) were made with anhydrous chlorobenzene (Sigma-Aldrich) in a N_2 glovebox. Solutions were stirred for a minimum of 12h and heated to 90°C for 5 min prior to use to ensure dissolution.

Solar cells (device area = 0.162 cm^2) were fabricated on indium tin oxide (ITO) coated glass substrates (Kintec, Hong Kong). The substrates were cleaned with Aquet detergent solution and water, followed by 10 min of sonication in acetone and 10 min in isopropanol, and 10 min of UV-ozone treatment. Poly(3,4-ethylenedioxythophene) poly(styrenesulfonate) (PEDOT:PSS) was spun cast in a laminar flow hood at 4000 rpm for 2 min and subsequently dried at 165°C for 10 min. P3HT/PCBM (24 mg/mL) active layers were spun cast in a N_2 glovebox at 1000 rpm for 1 min. A 75 nm layer of aluminum was deposited via thermal evaporation at 10^{-6} torr. Devices were then thermally annealed, cooled, and characterized, all while remaining under the N_2 atmosphere.

Electrical characterization of devices in the dark and under AM 1.5G (0.1 mW/cm^2) illumination from a 150W Newport solar simulator was performed using a Keithley 2636A Sourcemeter. All device testing took place in a N_2 glovebox. At least 6 devices were averaged for all of the data presented here.

Transmission Electron Microscopy (TEM) experiments were conducted on a JOEL 2010 at the Materials Research Institute of The Pennsylvania State University. Bright-field images,

elemental maps, and thickness maps were obtained. Elemental maps (carbon and sulfur) were obtained via the standard three-window method.[15] TEM samples were prepared by spin casting PEDOT:PSS in a laminar flow hood at 4000 rpm for 2 min followed by spin casting P3HT/PCBM (24 mg/mL) in a N_2 glovebox at 1000 rpm for 1 min. Films were next floated-off with distilled water and picked up with copper TEM grids. Samples were dried for 24 h under vacuum and then thermally annealed in a N_2 glovebox.

RR/RRa P3HT absorbance measurements were taken using a Beckman DU Series 500 spectrophotometer.

Chapter 3

Results and Discussion

Initial effects due to the introduction of RRa P3HT to the active layer are exhibited in the traditional manner of device characterization, current-potential curves (or J-V curves). As light is shone onto the device, a potential is applied in manner that either promotes the movement of charges out of the device (reverse bias) or resists the movement of charges (forward bias). For the latter case, the device is within a power generating regime in which the current developed from the incident light produces power. Typically, these devices are characterized by the current at which no bias is applied, or the short circuit current, J_{SC}, since this is the current we obtain for simply shining light on the device.

Many of these the curves for varying ϕ_{P3HT} across the phase diagram of **Figure 1-1** were gathered. Representative curves for pure RR P3HT, 50% RR and 50% RRa P3HT, and pure RRa P3HT for ϕ_{P3HT} within the miscible region of the phase diagram are shown in **Figure 3-1**. The curves shown depict a sharp decrease in the J_{SC} with the introduction of RRa polymer and the purely amorphous devices operate essentially as a resistor rather than a power producing device.

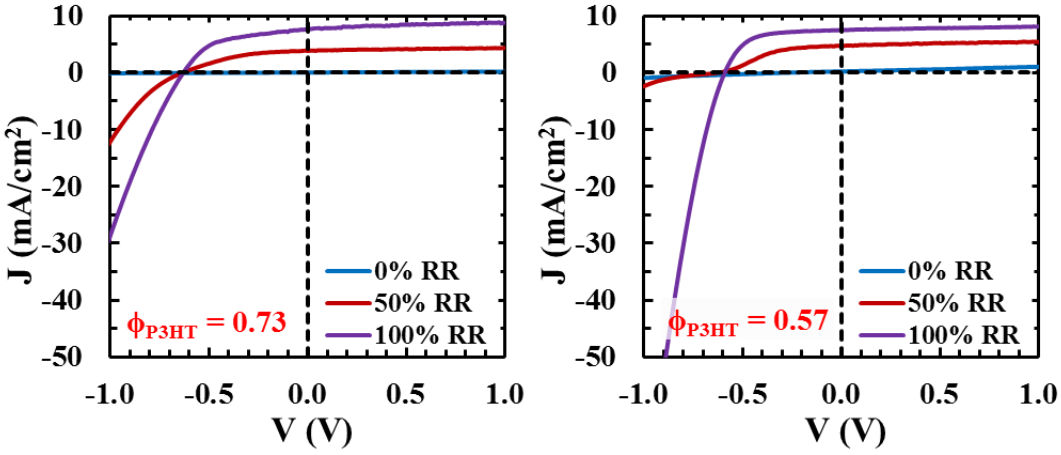

Figure 3-1. J-V Curves (miscible). The intersection of the curves and the vertical dashed line represent the J_{SC}. The devices experience significant decreases in J_{SC} upon the introduction of RRa P3HT.

However, as we move into the 2-phase region of **Figure 1-1**, we see this decrease in J_{SC} to be much less prominent. **Figure 3-2** contains representative curves for the same RR P3HT content but now for ϕ_{P3HT} below 0.42, thus what we predict to phase separate in the active layer. The introduction of amorphous polymer to these devices has much less of an effect on the J_{SC} and, in some cases, the difference between the pure RR and other curves is nearly indistinguishable. These initial observations agree with the previous findings represented in **Figure 1-2**, in which PCBM miscibility with the amorphous polymer has detrimental effects to charge mobility (and thus current).

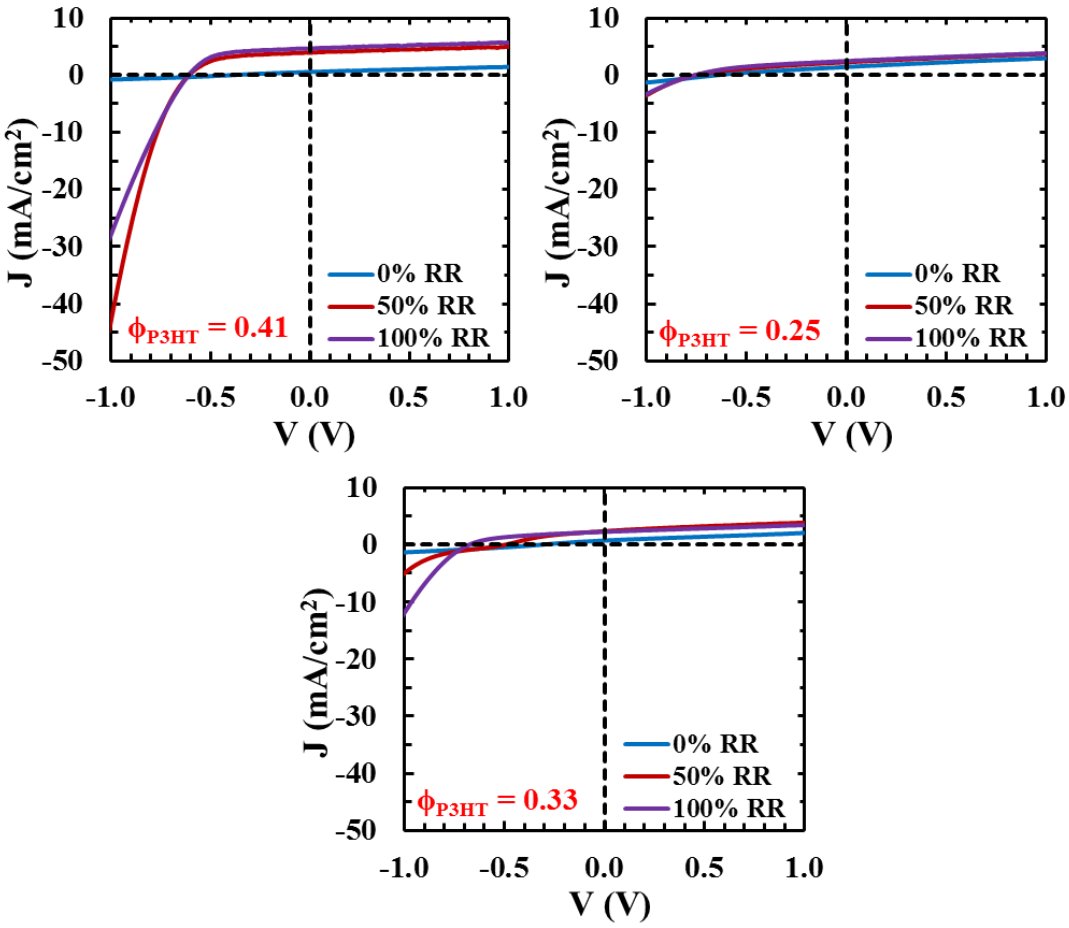

Figure 3-2. J-V Curves (2-phase). The intersection of the curves and the vertical dashed line represent the J_{SC}. The introduction of RRa P3HT to these devices has much less of an effect on the J_{SC} than higher ϕ_{P3HT}.

To gain a better appreciation for the effects of the amorphous polymer, we can analyze the change in J_{SC} for all the studied ϕ_{P3HT} as the RR content is modulated. **Figure 3-3** illustrates these effects for the ϕ_{P3HT} in the miscible region of the phase diagram. We again see that the introduction of the amorphous polymer has immediate consequences on device performance. Furthermore, the two polymer species appear to be operating independently of one another since the data deviates very little from a simple linear average of the devices composed of either pure polymer species (shown as the dashed line).

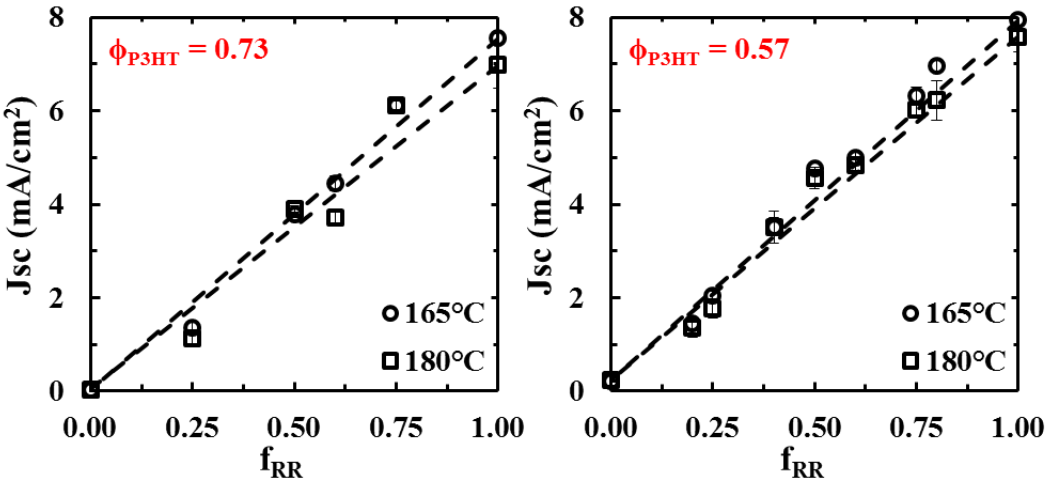

Figure 3-3. J_{SC} as a function of RR content (miscible). The introduction of RRa P3HT causes immediate and sharp decreases in the J_{SC}. The dashed lines depict a linear average between the two devices at f_{RR} = 0.00 and f_{RR} = 1.00 in order to distinguish any variations from the polymer species acting independently of each other. The results shown here suggest that RR and RRa P3HT do operate independently.

The same analysis is conducted for the lower ϕ_{P3HT} for which we predict the polymer/fullerene blend to phase separate. These results are illustrated in **Figure 3-4**. Similar to the observations of **Figure 3-2**, we see that the replacement of crystalline with amorphous polymer for these low ϕ_{P3HT} has much less of an effect on the J_{SC} of the devices. However, these plots clearly show that there is some deviation from independent behavior of the polymer species. In fact, the J_{SC} appears to be enhanced for mixtures of the RR and RRa polymer above what the polymer species should contribute independently.

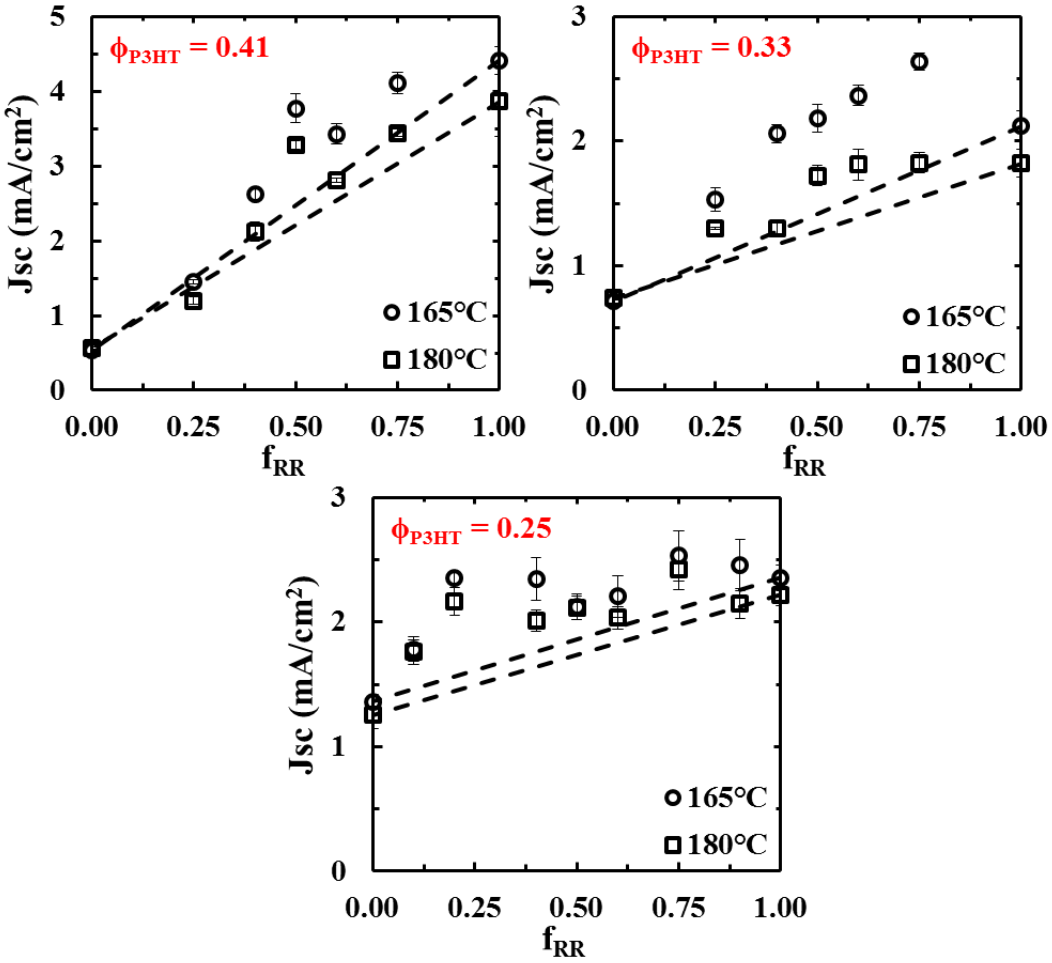

Figure 3-4. J_{SC} as a function of RR content (2-phase). The introduction of RRa P3HT has a lessening effect on the J_{SC} for the low ϕ_{P3HT}. The dashed lines depict a linear average between the two devices at $f_{RR} = 0.00$ and $f_{RR} = 1.00$ in order to distinguish any variations from the polymer species acting independently of each other. The results shown here suggest that RR and RRa P3HT do not operate independently and experience an enhancement above what would be expected from the individual polymer species.

Despite the fact that the J_{SC} of any given device should be indicative of the photocurrent through the device, we notice that these curves do not plateau for the top portion along which the J_{SC} sits. Our devices model imperfect diodes; ideal devices would see a constant current, the photocurrent, along all portions of reverse bias and some area of the forward bias until the applied potential overcomes the intrinsic device potential. At this point the current would immediately drop off to infinity. Thus, the J_{SC} here cannot be used as the device photocurrent. For this reason, we ask the question of how the photocurrent is being affected with the introduction of RRa P3HT.

In order to do this, we look to the current at the greatest reverse bias, an applied potential of 1V. This point represents the highest current that we are able to extract of the device and what should be achieved in the device if no charges are being trapped due to inadequate mobility. The current at 1V, then, is studied as the approximate photocurrent of the device. When we develop the photocurrent data in a similar manner as before, we obtain trends redundant of those observed with the J_{SC} as a function of regioregular content. **Figure 3-5** represents these curves for high ϕ_{P3HT} and again shows that introduction of RRa content to the devices has immediate and severe consequences.

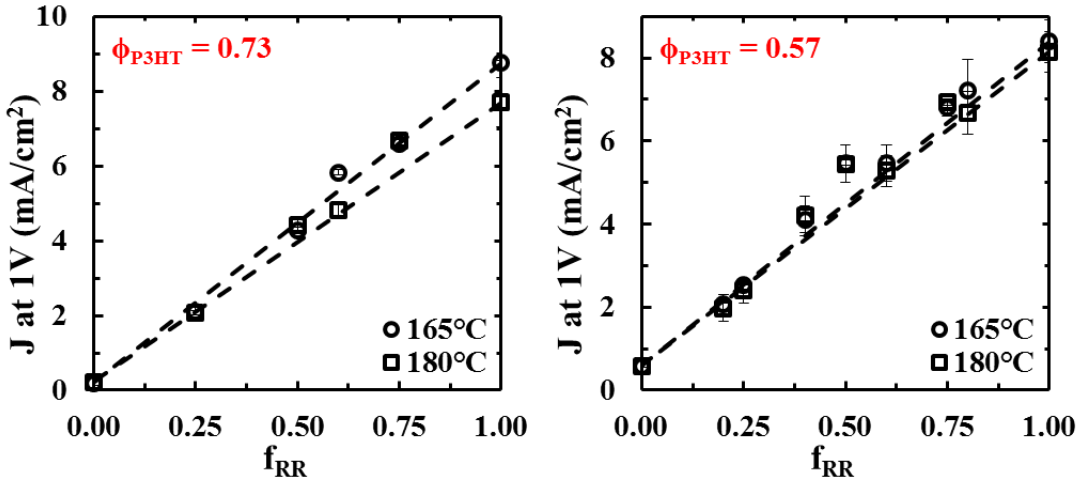

Figure 3-5. Photocurrent as a function of RR content (miscible). Again, the introduction of RRa polymer to the device causes immediate decreases in device performance. The two polymer species again appear to act independently of one another

Figure 3-6 illustrates the same analysis conducted for the low ϕ_{P3HT} that predict phase separation for an amorphous matrix. Yet again, we see the same trends as before; increasing RRa content appears to have a diminishing effect as ϕ_{P3HT} decreases and the data begins to deviate from the expected contributions of RR and RRa independently.

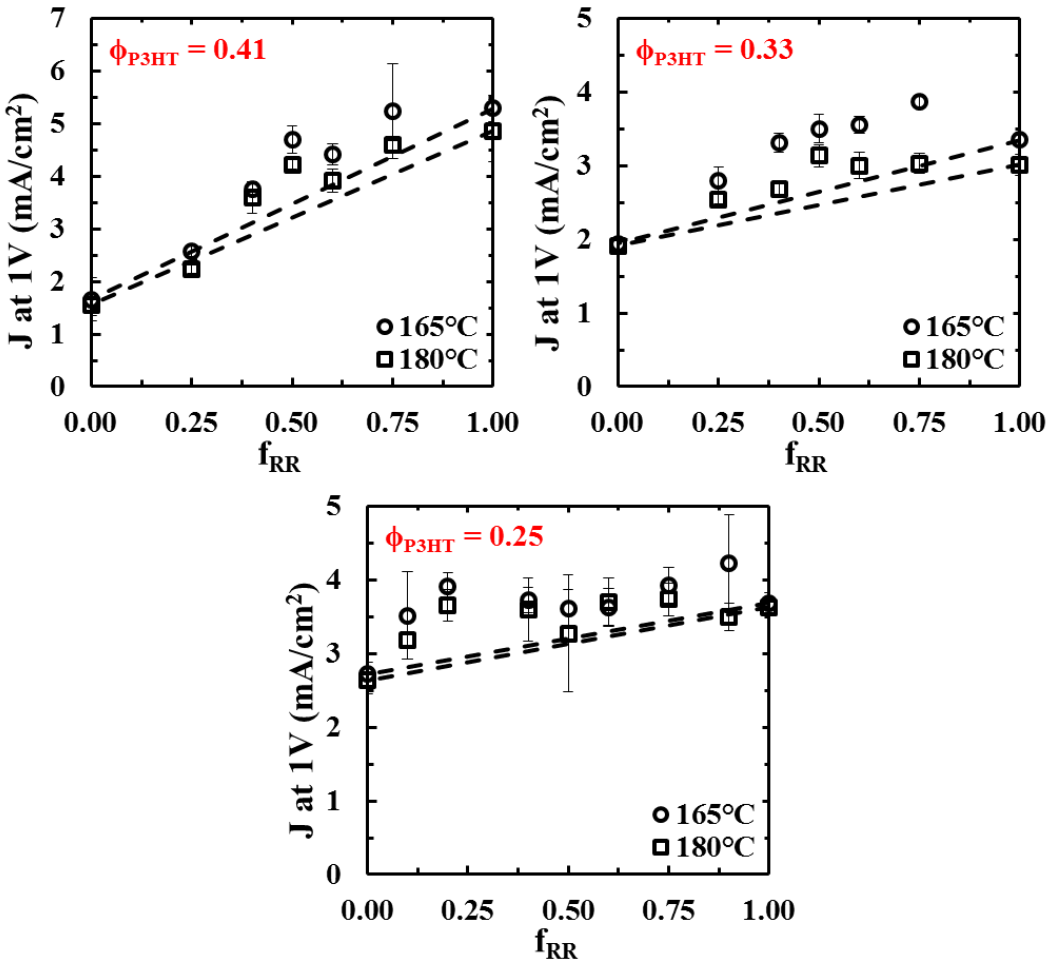

Figure 3-6. Photocurrent as a function of RR content (2-phase). Introduction of RRa polymer to these low ϕ_{P3HT} again causes little effects on device performance. The two polymer species deviate slightly from independent behavior.

However, to effectively analyze the photocurrent the absorption of the polymer species must be considered. The previous analysis of the J_{SC} applied to the photocurrent results in similar trends for the addition of RRa P3HT to the devices and would be redundant to show here. Instead, we examine the how the photocurrent is affected by considering that the introduction of RRa not only affects the charge transport through the device but also the thickness and absorbance of the active layer. **Figure 3-7** clearly depicts the diminished absorbance (with photon flux of the simulation environment) of the pure amorphous polymer over its crystalline counterpart. This significantly lower performance of RRa P3HT must be accounted for when

considering the effects that it has on device performance. Additionally, the thickness of the polymer fullerene layer must be considered since a thicker layer will absorb more photons, and vice versa.

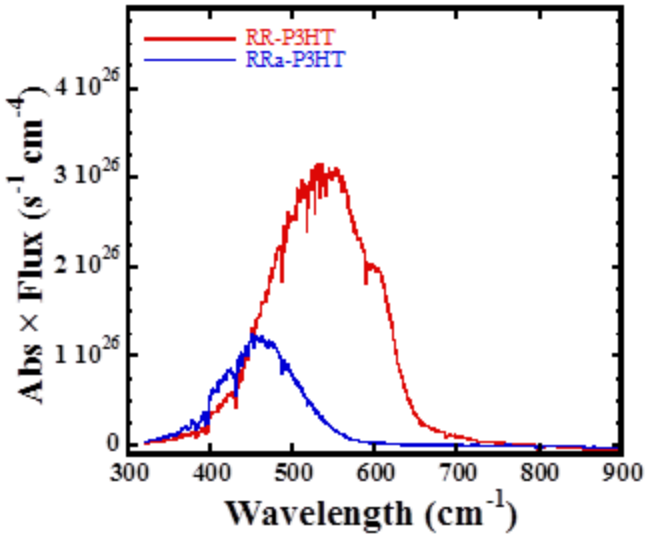

Figure 3-7. Photon Flux × Absorbance as a function of wavelength for RR and RRa P3HT.

We attempt to observe any readily apparent trends due to the absorption by mapping the number of incident photons captured by the devices as a function of RR:RRa content. That is, a relative absorption coefficient is obtained from **Figure 3-7** and observed as a product with device thickness for changing RR content. However, this analysis suggests that this absorption is an essentially monotomic function with increasing RR content. **Figure 3-8** depicts these findings.

Regardless of this initial lack of potential reasoning for the previously observed effects, we determine that the most effective route of analyzing the photocurrent and absorption manifests itself in an analagous measure of quantum efficiency; that is, the number of charges extracted from the device for the number of photons absorbed. This ratio is observed in a similar manner to the J_{SC} as a function of changing RR P3HT content. The results for the high ϕ_{P3HT} in the miscible region of the phase diagram are shown in **Figure 3-9**. We observe, again similar to previous analyses, that introduction of RRa polymer to the device decreases this parameter. However, for

these ϕ_{P3HT} that we predict to be miscible for the amorphous matrix, we see that the data deviates from what we would expect independent contributions to add up to.

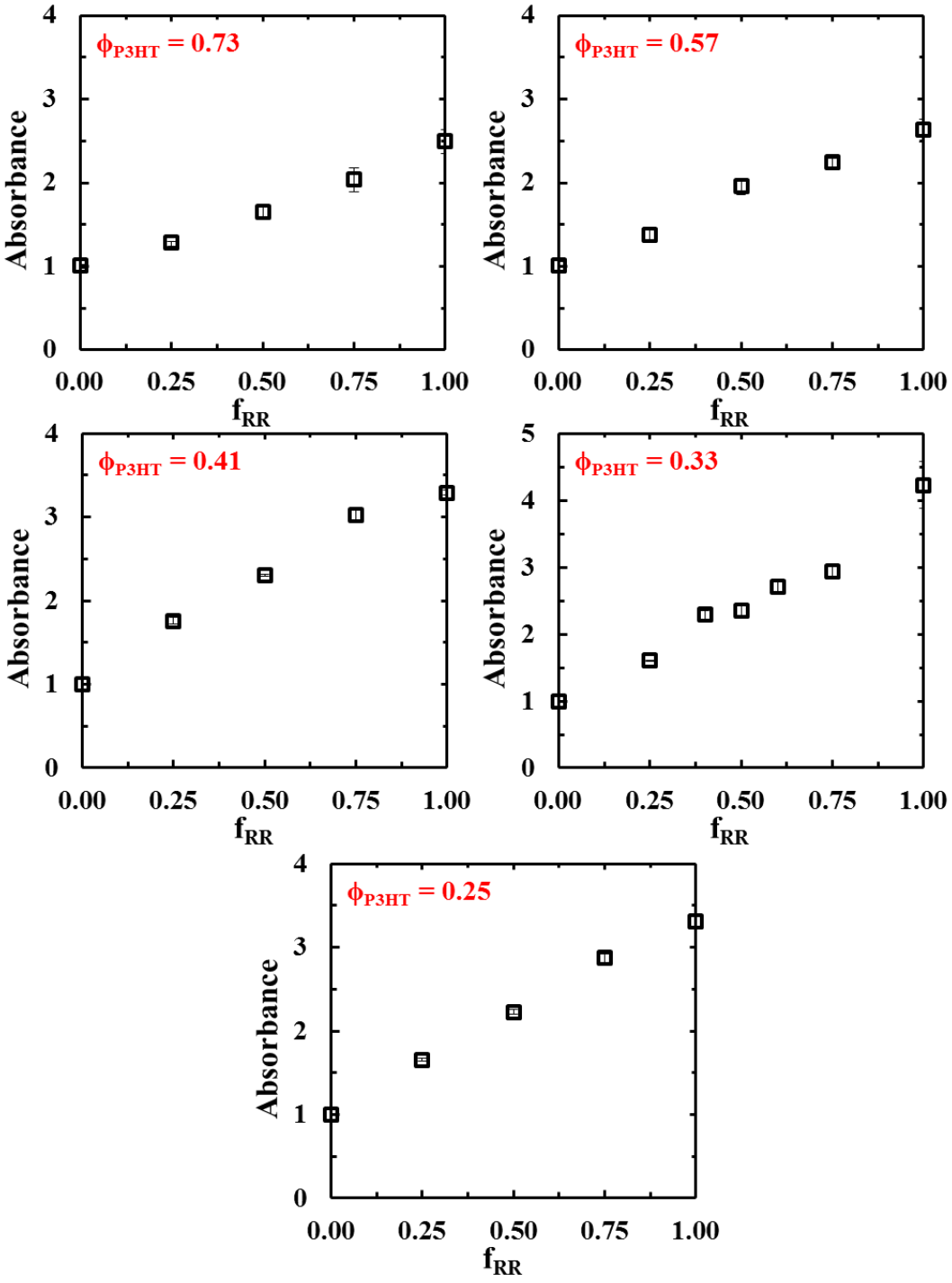

Figure 3-8. Photon Flux × Absorbance × Thickness. Trends in overall absorption appear similarly across all ϕ_{P3HT} and offer no explanation for previously observed trends in the J_{SC} or photocurrent data.

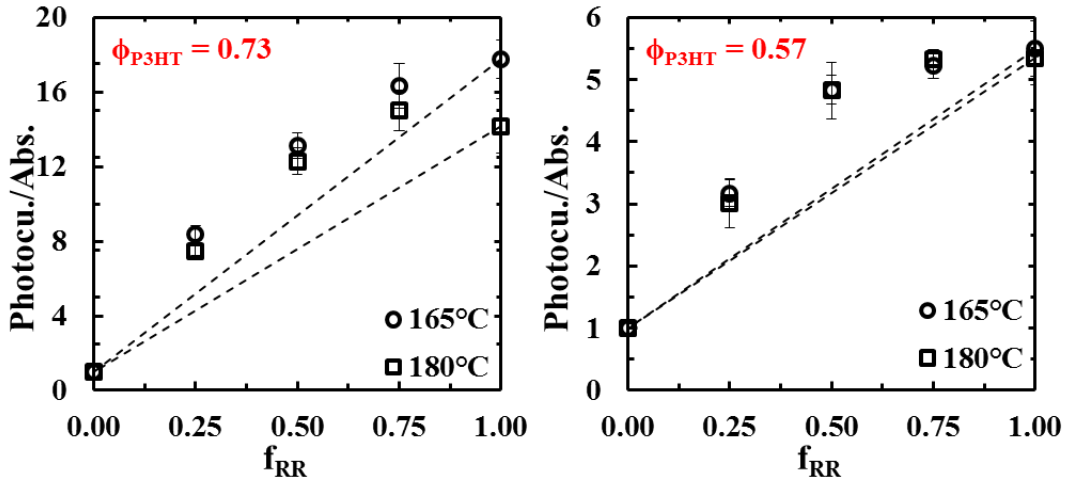

Figure 3-9. Photocurrent/absorption (miscible). Again, introduction of RRa polymer decreases the device performance; however, it is now seen that the two polymer species no longer appear to act independently for these high ϕ_{P3HT}.

These results are normalized (**Figure 3-10**) to best exhibit the variations from the independent contributions of the pure polymer species. We see that the photocurrent:absorption ratio deviates greatly from this independent behavior and strongly suggests that the mixing of the two polymer species has some synergistic effect for the miscible amorphous blends of P3HT/PCBM.

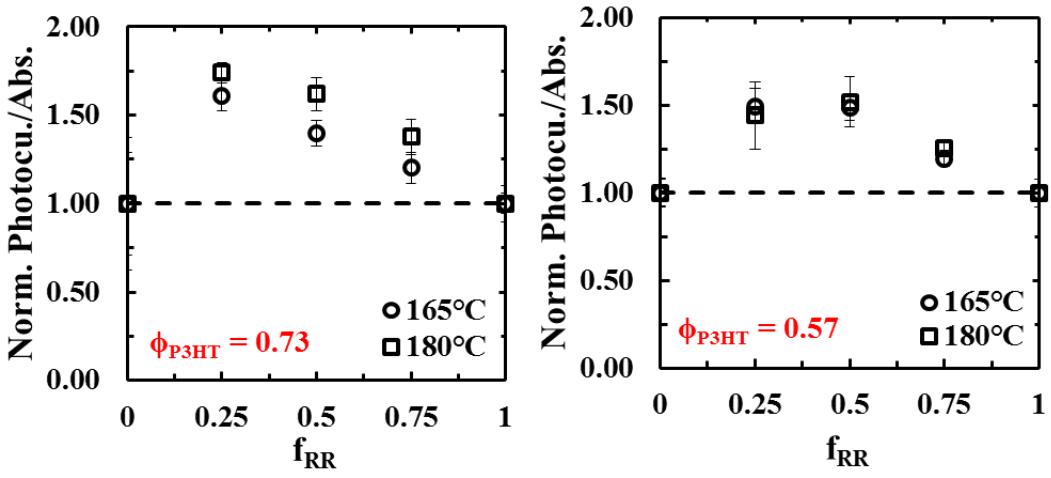

Figure 3-10. Normalized photocurrent/absorption (miscible). For these high ϕ_{P3HT}, it is easily seen that the two polymer species benefit from each other's presence and the device experiences a synergy and performance above what is expected.

Figure 3-11 represents the same analysis applied to the low ϕ_{P3HT} of the 2-phase region of **Figure 1-1**. In these instances the photocurrent:absorption ratio does not decrease as dramatically as for high ϕ_{P3HT}. In accordance with **Figures 3-9** and **3-10**, and unlike previous analyses for the J_{SC} and simple photocurrent, this data does not deviate from independent polymer behavior to any observable or meaningful extent. This suggests that the synergy experienced between the RR and RRa P3HT is only felt when the fullerene matrix surrounding the RR P3HT crystals in miscible with amorphous P3HT.

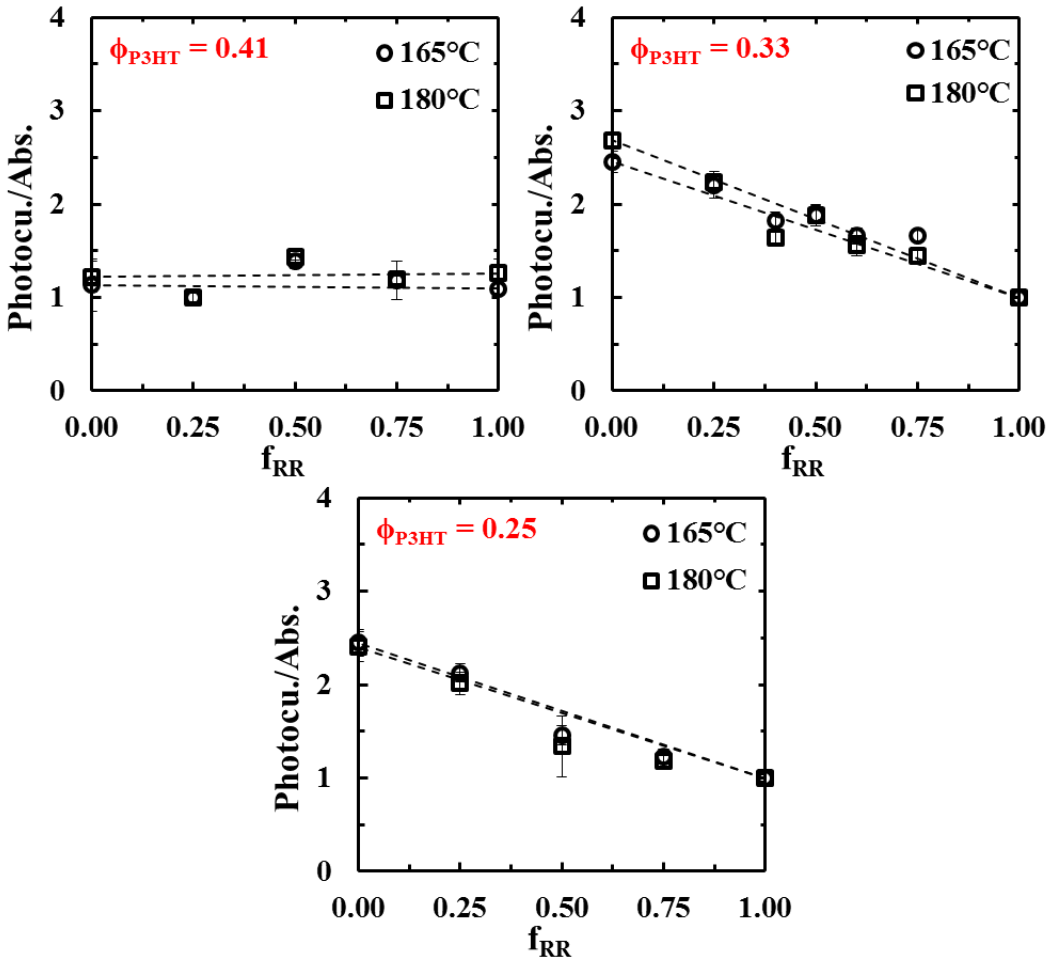

Figure 3-11. Photocurrent/absorption (2-phase). RRa polymer has a smaller effect on the devices in the 2-phase region of **Figure 1-1** and the polymer species now appear to act independently for these low ϕ_{P3HT}.

An interesting article between **Figures 3-9** and **3-11** is the shift from RR P3HT pure devices performing with a higher photocurrent:absorption ratio to RRa P3HT pure devices performing with a higher ratio. The suggestion that RRa P3HT operates better than RR P3HT (for this paramenter) for these low ϕ_{P3HT} is somewhat unprecedented and further work must be done to understand this phenomenon.

Again, the lack of deviation from independent performace is better exemplified through normalization of data and is illustrated in **Figure 3-12.**

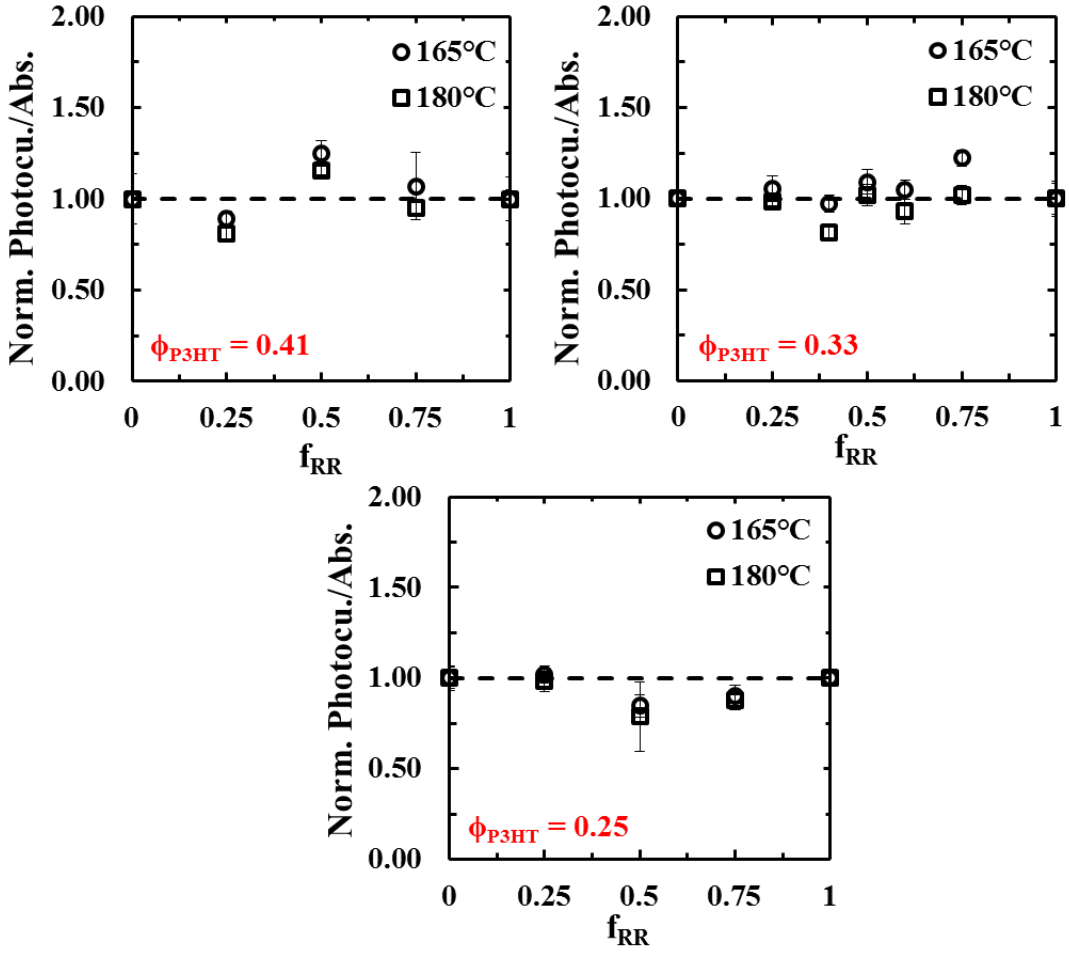

Figure 3-12. Normalized photocurrent/absorption (2-phase). For these low ϕ_{P3HT}, it appears that the two polymer species behave independently of one another and no synergy is experienced in the device.

In order to fully understand the effects that introduction of RRa P3HT has to the photocurrent and device performance, we utilize energy filtered transmission electron microscopy

(EFTEM). We predict phase behavior based on purely amorphous blends of P3HT/PCBM, and while this is a safe prediction for the blends of primarily RRa P3HT, any crystallization due to RR P3HT may have consequences beyond these predictions. EFTEM allows us to view elemental maps of nanoscale morphologies to better understand the anticipated changes made to morphology and better correlate the actual changes observed to the effects observed in device performance. We can further develop these elemental maps into composition maps that better show the relative volume fractions of P3HT and PCBM in localized areas. **Figure 3-13** shows this analysis for one ϕ_{P3HT} at 0.41, just inside what is predicted as a 2-phase blend. However, to effectively characterize the maps shown here we must develop further mapping of the various ϕ_{P3HT} observed in this study and correlate the relative changes in morphology to the device performances.

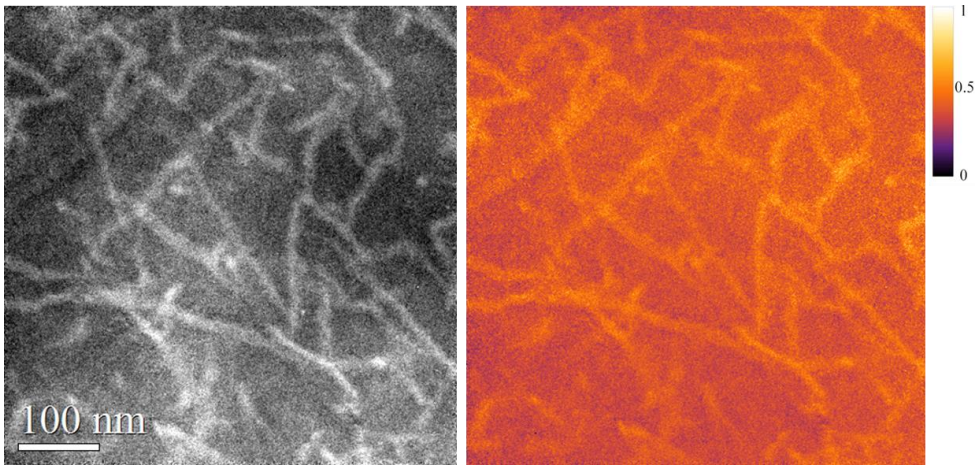

Figure 3-13. EFTEM Images. Sulfur elemental map (left) with corresponding composition map (right) for ϕ_{P3HT} = 0.41 and f_{RR} = 0.5. The scale bar for the composition map represents regions of higher sulfur content (white, 1 on the bar) and regions of high carbon content, i.e. PCBM (dark purple, 0).

Chapter 4

Conclusion

The results presented here suggest that miscible blends of P3HT/PCBM in OPV devices experience an enhancement with the introduction of RRa polymer to the fullerene matrix. This enhancement is viewed as a synergistic effect from the RR and RRa polymers working together rather than contributing independently to device performance. However, this synergy between the RR and RRa polymers is viewed only in light of the absorbance of the individual polymer species. In fact, device performance is diminished with the introduction of RRa polymer, indicating that charge transport of the RRa polymer, known to be very low, is the limiting factor of OPV devices that utilize this polythiophene/fullerene blend.

Further work is necessary to fully understand the results observed in the letter. Additional elemental mapping of the wide range of RR:RRa and Φ_{P3HT} will provide insight into whether the predicted changes made to active layer morphologies are obtained and representative of the hypothesis made here. These mappings may confirm the results here or suggest alterations to the observations seen with regard to how the fullerene matrix morphology changes with the introduction of RRa polymer. This is a vital consideration since RR polymer crystallization will affect the resulting equilibrium of the amorphous polymer/fullerene regions.

Additionally, the absorbance data used in this study is obtained from the transmission of the pure polymer species. This does not account for optical effects that may occur in the actual devices. The various layers and materials of OPV devices may lead to light trapping and varying absorptions for the different active layer blends. Comprehensive optical modeling will provide

absorbance data most indicative of the active polymers and show the accuracy of the absorbance data used in the current analysis.

BIBLIOGRAPHY

[1] Li, G.; Shrotriya, V.; Yao, Y.; Huang, J. S.; Yang, Y. J. Mater. Chem. 2007, 17 (30), 3126–3140.

[2] Brabec, C. J.; Gowrisanker, S.; Halls, J. J. M.; Laird, D.; Jia, S.; Williams, S. P. Adv. Mater. 2010, 22 (34), 3839–3856.

[3] Shaheen, S. E.; Ginley, D. S.; Jabbour, G. E. MRS Bull. 2005, 30 (1), 10–19.

[4] Thompson, B. C.; Fr_echet, J. M. J. Angew. Chem., Int. Ed. 2008, 47 (1), 58–77.

[5] Haugeneder, A.; Neges, M.; Kallinger, C.; Spirkl, W.; Lemmer, U.; Feldmann, J.; Scherf, U.; Harth, E.; Gugel, A.; Mullen, K. Phys. Rev. B 1999, 59 (23), 15346–15351.

[6] Shaw, P. E.; Ruseckas, A.; Samuel, I. D. W. Adv. Mater. 2008, 20, (18), 3516-3520.

[7] Campoy-Quiles, M.; Ferenczi, T.; Agostinelli, T.; Etchegoin, P. G.; Kim, Y.; Anthopoulos, T. D.; Stavrinou, P. N.; Bradley, D. D. C.; Nelson, J. Nat. Mater. 2008, 7, (2), 158-164.

[8] Xin, H.; Reid, O. G.; Ren, G.; Kim, F. S.; Ginger, D. S.; Jenekhe, S. A. ACS Nano 2010, 4, (4), 1861-1872.

[9] Kozub, D. R.; Vakhshouri, K.; Orme, L. M.; Wang, C.; Hexemer, A.; Gomez, E. D. Macromolecules 2011, 44, (14), 5722-5726.

[10] Vakhshouri, K.; Kozub, D. R.; Wang, C.; Salleo, A.; Gomez, E. D. Phys. Rev. Lett. 2012, 108, (2), 026601.

[12] Gomez, E. D.; Barteau, K. P.; Wang, H.; Toney, M. F.; Loo, Y.-L. Chem. Commun. 2011, 47 (1), 436–438.

[13] Burkhard, G. F.; Hoke, E. T.; Scully, S. R.; McGehee, M. D. Nano Lett. 2009, 9 (12), 4037-4041.

[14] Coffey, D. C.; Reid, O. G.; Rodovsky, D. B.; Bartholomew, G. P.; Ginger, D. S. Nano Lett. 2007, 7 (3), 738–744.

[15] Egerton, R. F., *Electron energy-loss spectroscopy in the electron microscope*. 2nd ed.; Plenum Press: New York, NY, 1986.

ACADEMIC VITA

Bryce Isaiah Edmondson
bryceedmondson@gmail.com

Education

The Pennsylvania State University – University Park, PA August 2009–Present

- B.S. Chemical Engineering with honors – Expected graduation in December 2013
- Schreyer Honors College Scholar
- 2013 Winner – The Larry Duda Undergraduate Research Award in Chemical Engineering
- 2013 Winner – The Lee and Mary Eagleton Award for Excellence in Design

Publications and Presentations

"Device Performance of Poly(3-hexylthiophene)/Fullerene Solar Cells Is Limited by Electron Transport" Edmondson, B.; Vakhshouri, K.; Kesava, S. V.; Rimshaw, A.; Rees, K. M. ; Asbury, J. B.; Gomez, E. D., to be submitted

"Device Performance of Poly(3-hexylthiophene)/Fullerene Solar Cells Is Limited by Electron Transport", Edmondson, B.; Vakhshouri, K.; Kesava, S. V.; Gomez, E. D.; Oral Presentation, The American Institute of Chemical Engineers Annual Meeting, San Francisco, California, November 2013.

Research and Laboratory Experience

Penn State Department of Chemical Engineering – University Park, PA December 2010– Present
Undergraduate Research Assistant, Dr. Enrique Gomez Research Group

- Investigated the performance of poly(3-hexylthiophene-2,5-diyl) (P3HT) and phenyl-C61-butyric methyl ester (PCBM) blends in organic photovoltaic devices. Specifically, studied the effects on charge transport due to regiorandom P3HT and concluded that charge transport is limited by amorphous regions of P3HT:PCBM blends.
- Fabricated and tested photovoltaic devices through use of a nitrogen glove box, spin coating devices, thermal evaporator, solar simulator, and ellipsometer. Characterized morphology of P3HT:PCBM blends through Energy Filtered Transmission Electron Microscopy (EFTEM).
- Synthesized block copolymers of styrene and isoprene monomers using an anionic polymerization method. Obtained experience in synthetic chemistry under vacuum conditions in addition to performing vacuum distillations and freeze drying products. Characterized polymers via gel permeation chromatography (GPC) and x-ray diffraction (XRD).

Research Experience for Undergraduates, University of Houston – Houston, TX May 2011 – July 2011
Undergraduate Research Assistant, Dr. Megan Robertson Research Group

- Synthesized copolymers of several acrylate (e.g. laurel and stearyl acrylate) monomers available from naturally occurring acids and oils as a preliminary step towards investigating the potential of using renewable resources for the creation of thermoplastic elastomer materials.
- Performed free radical polymerizations, atom transfer radical polymerizations (ATRP), and reversible addition fragment transfer polymerizations (RAFT).
- Characterized product polymers via nuclear magnetic resonance spectroscopy (NMR), differential scanning calorimetry (DSC), and gel permeation chromatography (GPC).
- Compiled Material Safety Data Sheets (MSDS) for all laboratory chemicals into a safety information binder to ensure laboratory safety.

Allegheny College Chemistry Department – Meadville, PA December 2008–May 2009
Chemical Stockroom Assistant

- Prepared chemical materials for use in organic chemistry laboratory exercises overseen by professors and practiced by approximately 100 students. Materials were prepared by stock solution dilutions, mixtures, titrations, or distillations.
- Gained experience working with concentrated acids, bases, and other hazardous chemicals and the proper handling protocols surrounding these dangerous materials.

Industry Experience

LORD Corporation – Erie, PA May 2013–August 2013
Elastomer, Adhesives and Coating Technology Student Intern

- Explored new and novel (and proprietary) classes of polymers as potential next-generation adhesive technologies for use in various aerospace and automotive applications. Specifically, synthesized new monomers and polymers with potential metal-to-rubber bonding capabilities and unique characteristics such as easily tailored curing temperatures, temperatures resistances, barrier properties, and economic advantages.
- Synthesized new monomer materials utilizing several different common chemistry reactions such as condensation reactions, Steglich Esterification reactions, and Diels-Alder reactions. Synthesized new polymer and copolymer materials via free radical polymerizations in bulk and in solution, emulsion polymerizations, and ionic polymerizations. Some of these reactions involved controlled feeds of reactants to a reaction vessel, jacketed reactors to control temperature conditions, acid traps, and nitrogen purges, and varied in size from 250 milliliters to 4 liters.
- Collaborated with an analytical team to characterize products via NMR, DSC, GPC, mass spectrometry, and thermal gravimetric analysis (TGA).

JOM Pharmaceutical Services, Inc. (Johnson & Johnson) – Somerset, NJ May 2012–December 2012
Clinical Supply Chain and Operations Co-op

- Identified cost discrepancies caused by system errors and led solution developments that resulted in cost savings of approximately $30,000 per year. Improved time efficiency by over 50% for monthly cost and metric reports by developing functional, macro-driven Excel applications. Developed standard operating procedures (SOP) for clinical trial closures.

Ainsworth Pet Nutrition – Meadville, PA May 2010–August 2010
Research and Development Student Intern

- Confirmed pet food safety by validating that final product nutrient profiles met the American Association of Feed Control Official's (AAFCO) compliance standards for dog and cat foods. Combined nutrient data from literature sources, contracted analytical laboratories, and in-house infrared spectroscopy (IR) to develop accurate profiles. Collaborated with a team of food scientists to address nutrient violations.

Organizations, Affiliations, and Extracurricular Activities

- Tau Beta Pi Engineering Honors Society
- American Institute of Chemical Engineers
- National Society of Collegiate Scholars
- National Multiple Sclerosis Society's "Bike MS"
- American Diabetes Association's "Tour de Cure"
- Schreyer Honors College Orientation Mentor
- Penn State Club Soccer